J Food Sci Technol (March 2021) 58(3):1081–1092
https://doi.org/10.1007/s13197-020-04622-z

ORIGINAL ARTICLE

Upgrading of agro-industrial green biomass residues from chocolate industry for adsorption process: diffusion and mechanistic insights

Amel Hamadi[1] · Nacera Yeddou-Mezenner[1] · Azeddine Lounis[2] · Rehab M. Ali[3] · Hesham Hamad[3]

Revised: 12 June 2020 / Accepted: 3 July 2020 / Published online: 15 July 2020

Abstract In the last decades, the world suffers from the wastes those results from unprecedented growth in the food industry. This context investigated the characteristics and suitability of utilizing cocoa shell (CS), an agro-industrial residual biomass waste from the chocolate industry, without any chemical and/or physical treatment. It is an abundant, low-cost, and green adsorbent that can be utilized for the effective removal of basic blue (BB41) as an example of cationic dye from aqueous solutions. The CS showed high adsorption potential (90.04%) with the mild operating condition, 45 min adsorption time, pH 6, CS dose 4 g/L, BB41 concentration 10 mg/L, stirring speed 400 rpm at 295 K. The kinetic, equilibrium, isotherms and mechanism studies revealed that the BB41 adsorption onto CS was attained mainly by electrostatic interaction, π–π stacking interaction, hydrogen bonding, covalent bond, and physical mechanisms. Besides, the organic functional groups played an important role during the adsorption process. The thermodynamic parameters suggested that the adsorption of BB41 dye was the non-spontaneous endothermic process with an activation energy 18.28 kJ/mol. From the industrial point of view, this work offers an economical push in waste management and also a green approach for the effective removal of toxic dyes from textile wastewater.

Keywords Green adsorbent characteristics · Agro-industrial biomass · Equilibrium studies · Adsorption mechanisms · Thermodynamic

Introduction

Nowadays, wide attention has been concerned with the lignocellulosic biomass owing to its distinctive characteristics such as cheapness, abundance, availability, renewable resources, environmentally friendly, biodegradability, etc. This biomass is produced mainly from the food industry and discharged without any valorization in addition to the incorrect disposal of some of them which lead to many environmental hazards. These residues are inedible, have high-value bioactive components, and have useful physicochemical properties which enable them to be effective adsorbents instead of considering them as wastes. Different agricultural residues have been utilized as adsorbents in their natural forms such as peanut hull (Ali et al. 2016), rice husk (Elhafez et al. 2017), seed hull (Khamparia and Jaspal 2017), coconut mesocarp (Monteiro et al. 2017), etc.

About 80% of all the cocoa fruit dry weight is the cocoa (*Theobroma cacao*) shell (CS) which is considered as a by-product in the chocolate industry. Thereby, CS represents a serious incorrect disposal problem and an untapped

Electronic supplementary material The online version of this article (https://doi.org/10.1007/s13197-020-04622-z) contains supplementary material, which is available to authorized users.

✉ Hesham Hamad
heshamaterials@hotmail.com; hhamad@srtacity.sci.eg

[1] Laboratory of Engineering of Reaction, Faculty of Mechanical Engineering and Process Engineering (USTHB), Algiers University of Science and Technology Houari Boumediene, BP 32, 16111 Bab-Ezzouar, Algeria

[2] Laboratory of Material Science and Engineering, Faculty of Mechanical Engineering and Process Engineering (USTHB), Algiers University of Science and Technology Houari Boumediene, BP 32, 16111 Bab-Ezzouar, Algeria

[3] Fabrication Technology Research Department, Advanced Technology and New Materials Research Institute (ATNMRI), City of Scientific Research and Technological Applications (SRTA-City), Alexandria 21934, Egypt

resource (Campos-Vega et al. 2018). Hence, it is a motivating topic for researchers to benefit from this environmentally friendly, abundant, and low-cost waste by the synthesis of valuable products from it. In addition to preventing the environmental elevated problems due to the wastes' improper disposal.

On the other hand, much attention has been placed upon dye removal from the textile industries' waste streams. Some researchers have focused on azo dyes as a result of their resistance to being treated. BB41 is a cationic azo dye that is significantly used for dyeing thread, carpets, wool and other textile materials. However, this dye is very toxic to aquatic life with long-lasting effects and can greatly affect the aquatic life that depends on photosynthetic activity due to the light penetration reduction. Therefore, BB41dye must be removed from industrial wastewaters using appropriate methods before discharging (Gupta et al. 2016).

Enormous techniques are utilized for dye removal from aqueous solutions but they mostly are complicated, ineffective and expensive, especially by applying them on a large scale. Besides, the conventional biological treatments, like the aerobic treatments, are not always effective for the textile industry wastewater as a consequence of the low biodegradability of many textile chemicals and dyes (Keskinkan and Göksu 2007). Adsorption treatment is a good alternative, promising, simple, cheap and effective technology to remove dyes and organic compounds from aqueous effluents (Ali et al. 2016; Elhafez et al. 2017).

Based on "wastes treat wastes" (El Essawy et al. 2017), this study aims to add value to CS (waste) by utilizing it as an adsorbent to remove BB41 dye (waste) from wastewater. To the best of our knowledge, this is the first study that investigates the effectiveness of raw CS in its natural form without any physical and/or chemical modifications for BB41 removal as a model of basic cationic dye from aqueous solutions. The target of this investigation is to study the equilibrium, kinetic aspects, and mass transfer limitations to evaluate and optimize the performance of the proposed low-cost adsorbent (CS). Various characterization techniques were utilized to investigate the changes between the fresh CS and dye-loaded CS characteristics. Different kinetic models i.e., pseudo-first-order, pseudo-second-order, intra-particle diffusion, and Boyd models were employed to simulate the adsorption under different dye concentrations. Moreover, the rate constants were evaluated and the rate-controlling step was identified. Furthermore, the adsorption isotherms and thermodynamic parameters were discussed to prove the CS feasibility and its high BB41 removal efficiency.

Materials and methods

Adsorbent

Cocoa shells (CS) used in this study were collected from BIMO chocolate Co. in Algeria (Fig. 1a). The shells were extensively washed several times with hot distilled water to remove the soluble organic impurities, dirt, dust and soil. Then they have been dried at 323 K in a furnace for 8 h. Completely dried CS was ground to powder by a mill and then sieved to select the desired particle size ($\leq$ 50 μm) that agreed with the literature (Ali et al. 2016) as shown in Fig. 1b. Some CS properties were determined such as; humidity 13.01%, ash content 13.25%, and density 0.488 g/cm^3.

Adsorbate

The BB41 was supplied by Fital Company, Algeria, and was used as received. The structure of BB41 and its modeling are shown in Fig. 1c and d, respectively. From Fig. 1c, BB41 is a basic cationic dye of azo type which has a methyl sulfate group with a negative charge.

Characterization techniques

The CS surface morphology features have been characterized by scanning electron microscope (SEM) provided with energy-dispersive X-ray spectroscopy (EDX) to detect the CS elemental structure (JEOL JSM 6360LA, Japan). These tests were performed at ambient temperature with an accelerating voltage of 20 kV. Fourier transforms infrared (FTIR) analysis was carried out using Shimadzu FTIR-8400 S, Japan. Where about 2 mg of the CS powder was mixed with 100 mg of KBr and ground in an agate mortar with pestle. The mixture was then pressed into a disc in a vacuum press at 80 KN. Measurements were conducted in a wavenumber range of 4000–400 cm^{-1}, with 4 cm^{-1} resolution to determine the functional groups that may affect the adsorption process (Jogihalli et al. 2017). The crystalline phases were analyzed using the X-ray diffractometer (Shimadzu-7000, Japan XRD). The patterns were recorded using copper K-alpha (Cu Kα) radiation (λ = 1.5418 Å) and step-scan mode [range: 5°–50° (2θ), step-time: 0.5 s, step-width: 0.1°]. The SEM, EDX, FTIR, and XRD investigations were conducted to the fresh CS and the CS after the adsorption process.

Batch equilibrium studies

Adsorption equilibrium investigations were studied in a batch mode by agitating CS with BB41 dye solution with

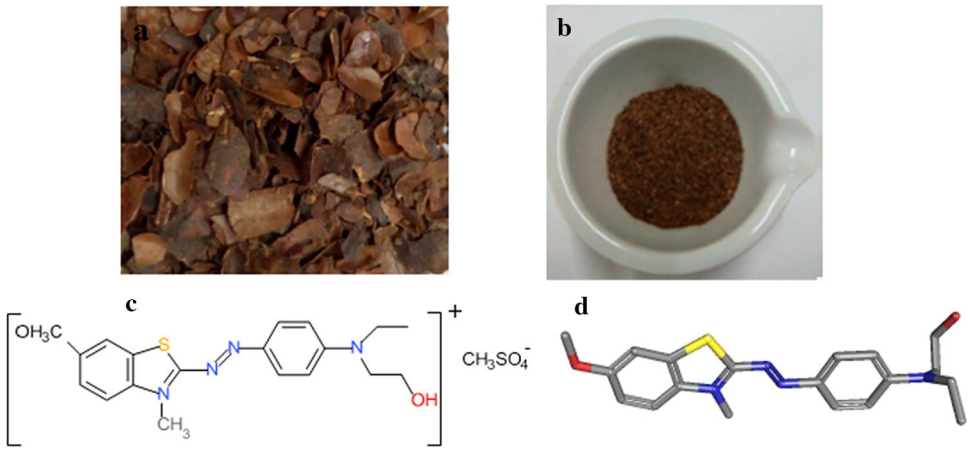

Fig. 1 **a** Cocoa shells obtained from chocolate company, **b** cocoa shell powder, **c** molecule structure of BB41 dye, and **d** modeling of BB41 dye

an initial dye concentration of the range from 5 to 25 mg/L at an agitation speed of 400 rpm. The effect of the contact time between the CS and the solution is evaluated during the period from 0 to 180 min. The influence of the solution temperature is investigated in the range from 295 to 323 K. The adsorption studies were conducted in triplicate for all analyzes and the mean values are presented in the figures. The influence of the CS dose on the adsorption process has been investigated at the range from 0.5 to 5 gm/L. All the batch experiments were performed at an initial solution pH 6 without any modification of the solution pH during the investigations. To study the effect of the solution pH on the adsorption process, the solution pH has been adjusted between 2 and 9 using 0.1 M HCl or NaOH. Centrifugation for 1 min at 5000 rpm has been conducted to separate the adsorbent from the solution. The residual dye concentration in the aqueous solution has been analyzed by spectrophotometer UV–Visible Spectroscopy (OPTIZEN 3220, Korea) at λ = 610 nm.

The BB41 percentage removal can be calculated using the following equation:

$$\%R = \frac{(C_0 - C_t)}{C_0} \times 100 \quad (1)$$

where %R is the BB41 percentage removal, C_0 is the initial BB41 concentrations in the solution, mg/L, C_t is the BB41 concentration at time t, mg/L.

The amount of adsorbed BB41 per unit weight of CS, q_t (mg/g), was determined using the following equation:

$$q_t = \frac{C_0 - C_t}{m} \times V \quad (2)$$

where q_t is the amounts of adsorbed BB41 after time t, mg/g, C_0 is the initial BB41 concentrations in the aqueous solution, mg/L, C_t is the BB41 concentration in the aqueous solution at time t (min), mg/L, V is the volume of the solution, L, and m is the CS weight, g.

Kinetic, isotherm and thermodynamic equations used in this study

The linear forms of kinetic models, linear and non-linear isotherm models, and thermodynamic parameters of removal of BB41 dye onto CS and statistical fits of the sorption data are given in supporting information (S1.1., S.1.2., and S.1.3., respectively).

Results and discussion

Characteristics of cocoa shells with an exploratory study of adsorption

Surface morphology and elemental analysis

Figure 2a and b show the surface morphology of CS before and after the adsorption process. Before the adsorption process, the surface of fresh CS is porous and rough which reflects the effective adsorption feasibility to the BB41 adsorption into the pores (Fig. 2a). The morphology shows that the fresh CS pores diameters are from 10 to 50 µm. After the adsorption process, the surface became smoother with the existence of very small residues that sealed the pores partially (Fig. 2b). Moreover, the dye coated the whole CS surface which became more compacted than the fresh CS. The surface morphology of the fresh CS and the CS after the adsorption process are completely different which articulate efficient dye adsorption at natural pH.

The chemical composition of CS is qualitatively and quantitatively determined by EDX. As expected, due to the plant nature of CS, there are high carbon and oxygen contents associated with traces of few elements like sulfur (S), calcium (Ca), nickel (Ni), phosphorus (P), aluminium (Al), sodium (Na), magnesium (Mg) and silicon (Si) (Fig. 2c, d). The CS high carbon content, about 75%, may

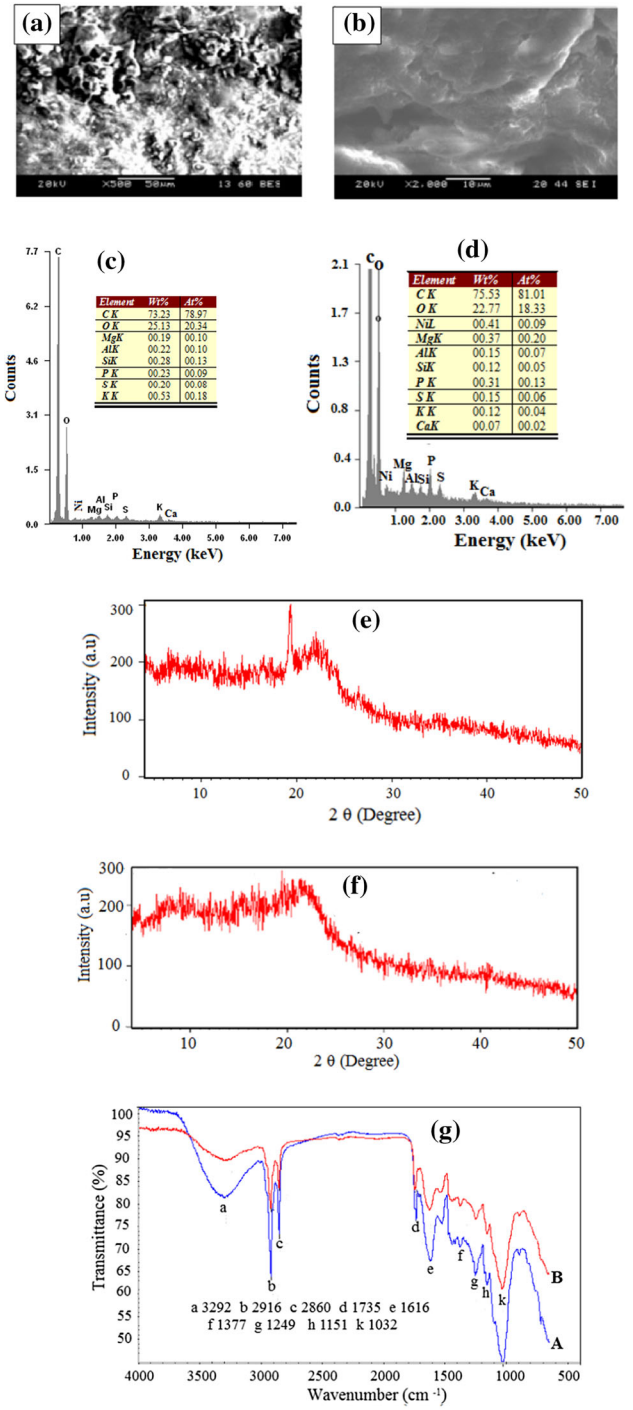

Fig. 2 SEM images of **a** fresh cocoa shells, **b** after adsorption, EDAX of **c** fresh cocoa shells, **d** after adsorption of BB41 dye, XRD of **e** fresh cocoa shells, **f** after adsorption of BB41 dye, and FTIR of **g** fresh cocoa shells (A), and after adsorption (B)

enhance the adsorption efficiency by the functional groups that attached to the carbon (Shokry et al. 2019).

Crystalline structure

The CS crystallinity changes were studied by XRD-patterns (Fig. 2e, f). Fresh CS showed a typical cellulose structure which has the main peak as indicative of crystalline cellulose with type II (Fig. 2e) (Hamad et al. 2018). After adsorption, the main crystalline peak of cellulose was missing which reflects the interaction of CS with BB41 and hence revealed the possibility of the BB41 adsorption onto CS (Fig. 2f).

Surface chemistry

Figure 2g shows the FTIR spectra which confirm the intensity reduction and/or broadening of the peaks after the BB41 adsorption onto CS. The broad bands at 3292 cm^{-1} indicate the stretching vibration of O–H functional groups on the CS surface (Hamad et al. 2018; Bassyouni et al. 2019). The symmetric and asymmetric stretching vibrations of C-H which are related to the presence of cellulose and hemicellulose are represented by the bands at 2916 and 2860 cm^{-1} (Hassaan et al. 2019). The C=O stretching of lactones, ketones, and carboxylic anhydrides are represented by the bands at 1735 cm^{-1} (Ahmad et al. 2015), whereas the bands at 1616 cm^{-1} are corresponding to rings mode of aromatic features. The bands at 1377 cm^{-1} are corresponding to carboxylic structure or alkyl groups (Ahmad et al. 2015). The bands at 1249 cm^{-1} are corresponding to C–O stretching in lignin and xylan (Ali et al. 2016). The bands at 1151 cm^{-1} with weak shoulders are assigned to Si–O–Si asymmetric stretching vibrations which were detected by EDX analysis (Hamad et al. 2015). The bands at 1032 cm^{-1} represent represents stretching vibration of the aryl –OH group in lignin (Kamel et al. 2018). The bands are shifted to lower wavenumbers after the adsorption process which confirms the sharing of these functional groups in the interaction between BB41 and CS. These results are confirmed with the investigations by SEM and XRD. Moreover, similar results are observed for adsorption of dye on the cupuassu shell (Cardoso et al. 2011), Citrus Limetta Peel, and Zea Mays Cob (Singh et al. 2017).

Adsorption study

Effect of the pH of the solution

The accessibility of functional groups such as hydroxyl and carbonyl and the degree of CS dissociation and ionization are greatly influenced by the pH of the BB41 solution and subsequently affect the adsorption efficiency (Ali et al. 2016). Figure 3a shows that the BB41 percentage removal increases from 73.32 to 90.04% by increasing the pH of the

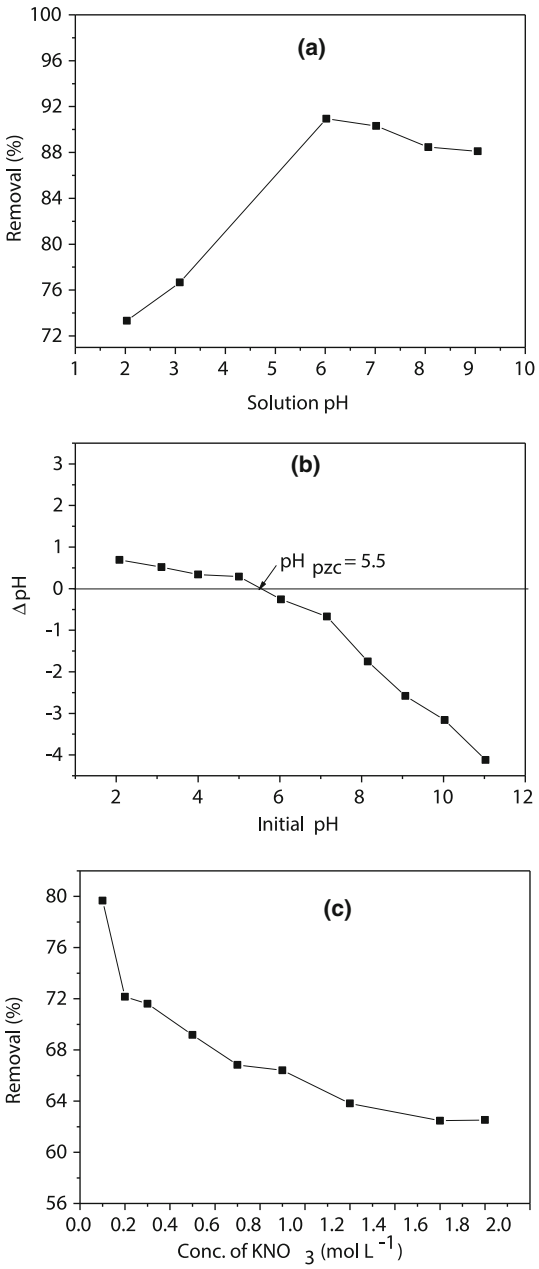

Fig. 3 **a** Effect of pH on the adsorption of BB41 dye, **b** variation of ΔpH versus initial pH for the determination of point of zero charge for CS, and **c** effect of ionic strength on BB41 dye removal by CS adsorbent. [Conditions; Co 10 mg/L, mass of CS of 4 g/L, stirring speed is 400 rpm, and T = 295 K]

BB41 solution from 2 to 6. The BB41 dye is a cationic dye therefore; it provides positive charges when it dissolved in water. A high concentration of protons is generated at pH $\leq$ 2, which strongly competes with cationic dye molecules of BB41 for the adsorption sites on the CS surface. This competition leads to BB41 percentage removal reduction from the aqueous solution. By increasing the pH, the electrostatic interaction between the negative charges of the CS adsorbent surface and the positive charges of the BB41 dye molecules is increased. This may occur as a result of increasing the deprotonation of the functional groups such as carboxylic and phenolic groups. Increasing the pH beyond 6 decreases the BB41 percentage removal slightly. This may be due to the reduction of the CS surface charge density which decreases the electrostatic repulsion between CS and BB41 and stabilizes the adsorption efficiency. These results are in agreement with the studies that reported in the literature for the adsorption of the cationic dyes onto the lignocellulosic adsorbents (Singh et al. 2017; Kooli et al. 2019).

Point of zero charge

Due to the CS nature, any variation in the operating pH condition can affect the CS surface charge. Moreover, the ionization constant (pKa) of the dye is important as it has a profound effect on the physicochemical properties of BB41. Hence the pH_{pzc} and pK_a determination is important to determine the pH effects on the adsorption process and determine the optimum operating pH.

Based on the point of zero charge (pH_{pzc}) of CS adsorbent and pK_a value of BB41 dye, the pH_{pzc} of CS is 5.5 (Fig. 3b) and pK_a of BB41 is 2.64. The BB41 dye molecule is at the molecular form at pH < pK_a while it is dissociated at pH > pK_a. Furthermore, at pH < pH_{pzc}, the CS surface is positively charged, whereas, at pH > pH_{pzc}, it is negatively charged. As the maximum BB41 removal efficiency (90.04%) has been reached at pH 6, the electrostatic interaction is the main mechanism of the adsorption process. At this pH, the CS is negatively charged (pH_{pzc} = 5.5) and BB41 dye is dissociated (pK_a = 2.64). Thus, the BB41 cations move towards the CS surface negative charges through electrostatic interaction. Similar results are reported in previous literature that investigated the removal of the cationic dyes using lignocellulosic biomass (Singh et al. 2017; El Essawy et al. 2017). Therefore, a further increase in pH did not enhance the surface charge intensity and also adsorption efficiency. By increasing the pH of the solution from 6 to 9, the BB41 percentage removal is decreased, indicating that the electrostatic mechanism is not the only mechanism that controlled the BB41 dye adsorption onto the CS adsorbent system.

Ionic strength

As it is expected, the ionic interactions play an important role in removing BB41 dye from aqueous solutions using CS as shown in Fig. 3c. The removal efficiency decreases with increasing the ionic strength of the dye solution. The removal efficiency decreased from 79.67 to 62.5% in the medium of KNO_3 that supporting the strong contribution of

the ion exchange mechanism of this adsorption process (Lim et al. 2016). Counter ions in the medium that surround the adsorption sites lose their charge and weaken the binding forces by electrostatic interaction between adsorbent and dye. The optimization of biosorption process is illustrated in Fig. S1 as mentioned in the following "Effect of cocoa shell dosage on the adsorption process", "Possible mass transfer limitations in the adsorption process" and "Adsorption kinetic studies" sections.

Effect of cocoa shell dosage on the adsorption process

Figure S1(a) shows a significant enhancement of the removal efficiency by increasing the CS dose from 0.5 to 4 g/L. This may be related to the existence of a greater number of active sites on the CS surface for BB41-CS interaction. Increasing the CS dosage than 4 g/L leads to remarkable removal efficiency reduction which indicates a reversible adsorption mechanism (Conrad et al. 2015). Hence, the 4 g/L can be considered as the optimum CS dose of BB41 removal.

Possible mass transfer limitations in the adsorption process

The study of external and internal mass transfer limitations was observed based on stirring speed and particle size distribution, respectively (Singh et al. 2017). The resistance of external mass transfer is investigated by changing the stirring speed from 100 to 600 rpm at contact time 45 min as shown in Fig. S1(b). Increasing the agitation speed slightly increased BB41 removal efficiency. The removal efficiency slightly increased from 86.32 to 90.94% by increasing the agitation speed from 100 to 400 rpm at 45 min contact time. Therefore, 400 rpm is the maximum removal efficiency for BB41 dye to reduce the resistance of external mass transfer. On the other hand, the resistance of internal mass transfer is proposed to be negligible in our study due to the very fine CS particle size ($\leq$ 50 µm).

Adsorption kinetic studies

Effect of agitation time

The effect of agitation time on BB41 removal is studied at different time intervals ranging from 0 to 180 min as shown in Fig. S1(c). There are two stages during the adsorption process. The first stage (first 15 min) shows a rapid BB41 removal which may be a result of the initial occupation of the most vacant sites and the availability of the active site of the adsorbent surface (Conrad et al. 2015). The second stage (within 15–45 min) shows a slow BB41 removal associated with gradual adsorption capacity which may be a result of the low remaining vacant sites on the CS surface in addition to the difficulties that obstacle the BB41 molecules against diffusion into the interior CS surface. The high chance of dye to bind with the functional groups (that determined in FTIR) leads to the first stage. Moreover, at the first stage, the CS external surface is filled by BB41 that leads to higher adsorption capacity.

Batch kinetic studies

The linear regressions of the kinetic models are expressed in "Kinetic, isotherm and thermodynamic equations used in this study" section. The fitting of experimental data with the kinetic models is illustrated in Fig. S2 and the constants are listed in Table 1. Pseudo-second-order kinetic model (Fig. S2(b)) has a higher R^2 value, superior to 0.99, at various initial dye concentration (C_o) with higher R^2 as compared with the pseudo-first-order model (Fig. S2(a)). Hence, this model suggests that the sorption process is controlled by chemical adsorption (Elhafez et al. 2017). The rate-limiting step of this chemical adsorption includes the valance forces by sharing or exchanging electrons between BB41 and CS surface that proved by the linear fitting with the Elovich kinetic model (Fig. S2(c)).

Table 1 Kinetic parameters for the adsorption of BB41 onto cocoa shell

Kinetic models	Initial concentration (mg/L)				
	5	10	15	20	25
Pseudo-first-order					
K_1 (min^{-1})	0.012	0.008	0.068	0.157	0.087
q_e (mg/g)	0.106	1.102	0.362	0.539	0.821
R^2	0.921	0.789	0.846	0.915	0.949
Pseudo-second-order					
K_2 (g/mg/min)	3.815	0.423	0.564	0.530	0.292
q_e (mg/g)	1.128	2.262	3.546	4.736	5.845
R^2	0.999	0.998	0.999	0.99	0.999
Elovich					
β (g/mg)	66.66	7.462	6.172	5.465	3.105
α (g/mg/min)	0.062	0.233	0.120	0.055	0.128
R^2	0.958	0.917	0.859	0.870	0.919
Intraparticle diffusion					
K_{id} (g/mg/min)	0.008	0.073	0.083	0.094	0.168
R^2	0.968	0.845	0.691	0.697	0.757
Boyd					
R^2	0.922	0.789	0.847	0.915	0.950

Mass transfer evaluation

To design the batch adsorption process, it is essential to analyze the mass transfer as a prediction of the adsorption process mechanism. Generally, there are many steps for the determination of mass transport of solute molecules across the phase boundary taking into account, the slowest step which is the rate-controlling step of the transport process. To realize the rate-limiting or controlling step, different mass transfer models such as intraparticle diffusion and the Boyd model have been applied to the experimental adsorption data (Thirunavukkarasu et al. 2018).

Intraparticle diffusion model The intraparticle diffusion model equation has been applied to evaluate the mass transfer (diffusion) process involved in the adsorption process. Figure 4a shows the plot of q_t versus $t^{0.5}$, where t is the contact time (min) and the parameters are summarized in Table 1. According to the curves, it can be assumed that there are three successive stages; external mass transfer, pore diffusion, and controlled reaction process which indicate that the adsorption processes have more than one adsorption rate (Adebayo et al. 2014). According to the SEM investigation in "Adsorption study" section, CS is a porous material; hence, it is urgent to analyze the role of pore diffusion to determine the rate-limiting step of the adsorption process.

The fastest sorption stage which is presented by the first linear segment does not pass through the origin in the initial phase (4 min). It refers to the strong interaction between BB41 and the external CS surface which can be devoted to the film diffusion (Roy et al. 2013). It could be elucidated by the reason of the electrostatic between BB41 and organic functional groups existed at CS is commonly considered to be fast and leads to higher removal in a few minutes. In the second stage, the BB41 molecules entered into the CS internal pores by intraparticle diffusion that represented by the second part of the plot (Ali et al. 2016). In the third segment region, no signified diffusion of BB41 onto the adsorption sites has occurred as a result of small pore diffusion, which is followed by an equilibrium (Banerjee et al. 2016). Therefore, it has been concluded that the BB41 removal using CS green adsorbent can be elucidated by film and pore diffusion mechanisms. In the present work, the experimental data fitting and R^2 values prove that film diffusion is the main mechanism with higher fitting and higher R^2 values than pore diffusion.

The liquid film diffusion model The main controller in the batch adsorption system is the boundary layer effect that determines the transfer of the solute molecules from the bulk liquid to the solid surface. Boyd model is utilized to predict the actual rate-determining step by investigating the

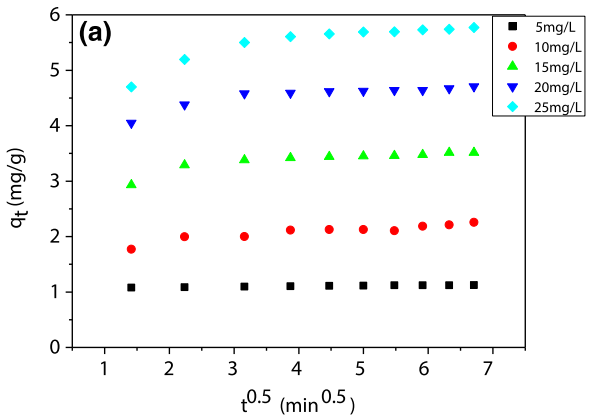

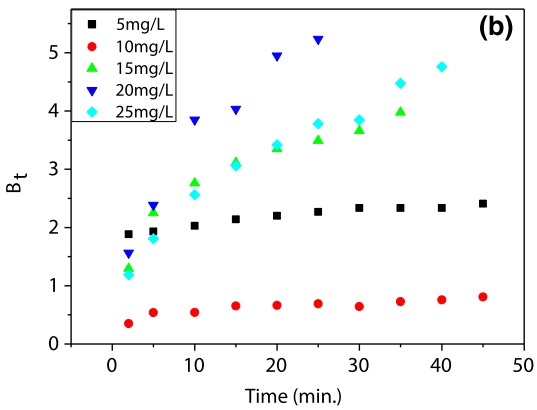

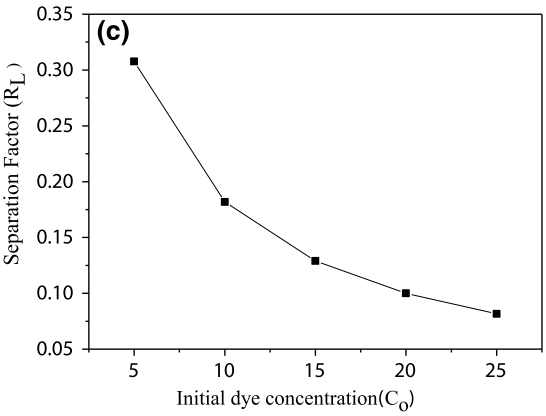

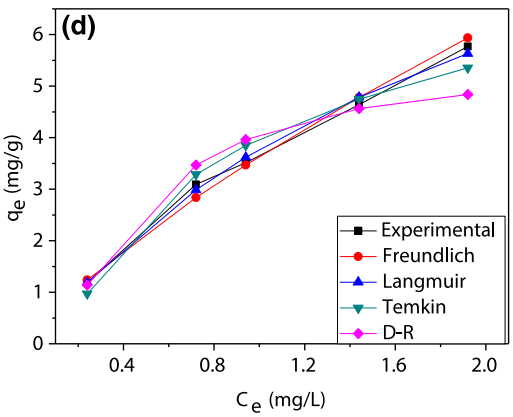

◀**Fig. 4** Kinetic plots of **a** intraparticle diffusion and **b** Boyd model, **c** R_L, and **d** non-linear equilibrium isotherm for the removal of BB41 by cocoa shell [Conditions; Co 10 mg/L, mass of CS of 4 g/L, pH = 6, stirring speed is 400 rpm, and T = 295 K]

role of the liquid film diffusion to the overall mass transport of the system that is shown in Fig. 4b. Linear lines that do not pass through the origin and the scattered points suggested that the BB41 adsorption onto CS is mainly controlled by external mass transfer, intraparticle diffusion, liquid film diffusion which proves the high affinity towards the adsorption process (Wang et al. 2018).

In conclusion, the experimental results of the adsorption process followed the pseudo-second-order model and the Boyd model. The applicability of these two models indicated that the BB41 adsorption onto CS is very complex and involved more than one mechanism.

Batch equilibrium studies

The adsorption equilibrium data is traditionally represented by the study of the initial concentration of BB41 and adsorption isotherms that presented in Fig. S3.

Effect of initial BB41 concentration

Figure S3(a) shows that BB41 removal efficiency is increased by decreasing the initial BB41 concentration. The removal efficiency decreased from 94.43 to 79.04% by increasing BB41 concentration from 5 to 25 mg/L at 45 min. This may be related to the following causes; (1) constant CS amount but increased BB41 concentration leads to a decrease in the ratio of available binding sites to initial BB41 concentration, (2) longer time of adsorption process is needed at the BB41 higher concentrations as a result of difficulties during the adsorption process three main stages; (i) movement of BB41 dye molecules to the boundary layer on CS adsorbent, (ii) diffusion into the boundary film layer and (iii) diffusion into the porous structure of the adsorbent (Pua et al. 2013) and (3) Dye tends to agglomerate which may reduce the adsorption rate. All adsorption experiments reached equilibrium within 45 min.

Equilibrium isotherms and adsorption interaction

The parameters of Langmuir, Freundlich, Temkin, and D-R isotherms are determined from the gradient and intercept of the linear models shown in Figure S3((b)–(e)) and the parameters have been summarized in Table S1.

The high R^2 values suppose a suitable model for the adsorption process explanation. From Table S1, the R^2 values obtained from Langmuir isotherm (0.998) are found to be closer to the one in comparison with the R^2 values of Freundlich isotherm (0.99). The value of 1/n is lower than 1 which confirms the heterogeneity of the adsorption process, which also is favorable and indicates a chemical adsorption process (Elhafez et al. 2017).

The investigated CS has good efficiency for this dye, compared to other adsorbents. Table S2 shows the adsorptive capacity of various adsorbents for the selected basic dyes. The CS exhibited the highest removal amount because they were not calcined and used as received.

In another way, the R^2 value of the Temkin isotherm model was > 0.95 which proves the uniform distribution of binding energies, up to some maximum binding energy and the indirect adsorbent-adsorbate interaction, when the BB41 molecules coated the CS surface as shown in SEM (Fig. 1b) (Singh et al. 2017).

Moreover, the high R^2 value of the D-R model suggests the chemisorption process of this study. The low free energy calculated from Eqs. 13 and 14 indicate that the BB41 adsorption mechanism onto CS is physical adsorption process as well due to electrostatic or Van der Wall's attractions.

The separation factor is an essential characteristic of Langmuir isotherm to detect the possibility of the adsorption process. It is calculated using the following equation and plotted in Fig. 4c.

$$R_L = \frac{1}{1 + bC_0} \tag{3}$$

where R_L is the separation factor, b is the Langmuir constant and C_0 is the initial BB41 concentration.

The R_L values are originated to be in the recommended range of favorable adsorption, i.e., $0 < R_L < 1$ at room temperatures for all different initial BB41 concentrations. Moreover, it is shown that the less favorable adsorption has occurred at high initial dye concentration because the R_L value is near to zero by increasing C_0. The high value of K_L (Langmuir equation) and the low value of R_L confirm the high solute/adsorbent adsorption interaction (Ahmad et al. 2012).

Moreover, the various error functions of the non-linear regression analysis are applied in this work to find out the best-fit isotherm model to the experimental equilibrium data. In this work, six different error analysis has been determined; sum of the square of the error (SSE), sum of the absolute error (SAE), average relative error (ARE), hybrid fractional error function (HYBRID), Marquardt's percent standard deviation (MPSD), Coefficient of determination of the linear regression analysis (R^2). All equations utilized for applying these models are mentioned in Eqs. (16–20) (Kumar and Sivanesan 2006).

The comparison of error values reflected that the error of Langmuir isotherm is significantly less as compared with Freundlich isotherm as indicated from Table S3 and Fig. 4d. This means that the Langmuir model is more suitable than the Freundlich model to explain the BB41 adsorption process onto the CS surface. This reflects the homogenous distribution of active sites onto the CS surface. The lowest error values are estimated from applying both Langmuir and Freundlich isotherms. Hence, these isotherms are considered as the best for describing the equilibrium of BB41 adsorption onto the CS surface.

Thermodynamic studies

The thermodynamic studies for biosorption of BB41 into CS sorbent are presented in Fig. S4 as follow;

Effect of solution temperature on adsorption of dye

Figure S4(a) shows a significant increase in the removal efficiency with the solution temperature increase from 295 to 303 K. This slight increase of the solution temperature enhances the BB41 removal rate which may be attributed to the improvement of the BB41 molecules diffusion rate into the CS internal pores and across the external boundary layer (Ahmad et al. 2015). Above 303 K, the removal efficiency is increased than in the case of 295 K while it is still lower than the removal efficiency at 303 K. These results prove that the BB41 adsorption onto CS is an endothermic process (Elkady et al. 2019). The adsorption capacity values are 3.093, 2.306, 2.29, and 2.306 mg/g at solution temperatures of 295, 303, 313, and 323 K, respectively. These values demonstrate that the BB41 adsorption process onto CS can be conducted at a moderate temperature (303 K) which is economic and save energy.

Activation energy parameters

The pseudo-second-order rate constant (k_2) is used for measuring the activation energy by Arrhenius Equation that presented at Eq. 21. Figure S4(b) shows the plot of ln k_2 versus 1/T to calculate the E_a. The value of activation energy (E_a) for BB41 adsorption onto CS is estimated to be approximately 18.28 kJ/mol. This value indicates that chemical and physical adsorption mechanisms are occurred according to the literature (Lim et al. 2016).

Thermodynamic parameters

From Fig. S4(c), ΔH° is estimated from the gradient and ΔS° is estimated from the intercept of the ln K_d versus (I/T) plot. Table S4 summarizes the thermodynamic parameters at different solution temperatures ranging from 295 to 323 K. The ΔH° positive value demonstrated the endothermic character of the BB41 adsorption process. Furthermore, the ΔS° positive value confirmed the enhanced randomness and disorder character at the solid–liquid interface. These results agree with the conclusion of the influence of agitation speed (as described in Possible mass transfer limitations in the adsorption process" section) and subsequently reflect the favorable condition of BB41 removal onto CS.

The water coordinated molecules are dislodged by BB41 molecules thereby increasing the transitional ΔS° than is missing by BB41 molecules which attribute to more randomness between BB41 and CS interaction (Kyzas et al. 2013).

The ΔG° negative values indicated that the BB41 adsorption onto CS is feasible, thermodynamically stable, and spontaneous (Elhafez et al. 2017). This spontaneity increases by increasing temperature which depicted the favorable BB41 adsorption at a higher temperature than room temperature. The negative and high value of ΔG° confirmed spontaneous and chemical adsorption, which is consistent with electrostatic interaction between BB41 and CS (Pua et al. 2013).

Suggested adsorption mechanism

The adsorption mechanism is necessary to understand the adsorption behavior of the BB41 dye onto the CS surface. The mechanism can also summarize the BB41 percentage removal that resulted from varying the different operating parameters, kinetics, isotherms, and thermodynamics. The above characterizations studies prove that the BB41 adsorption onto the CS was a complicated process, including several stages and various interactions. The suggested mechanism diagram is displayed in Fig. 5a.

Based on the results of BB41 models, the adsorption process can be split into a fast stage and a slow stage. The fast stage can be described by the electrostatic (ionic) interaction between the C–O, –OH, and –COO functional groups that presented on the CS surface and can anchor sites of basic BB41 dye and lead to high removal in few minutes. This interaction can be considered as the main adsorption mechanism (Islam et al. 2018). These results were consistent with the FTIR results, which showed a shift in the organic functional groups after the BB41 adsorption onto CS.

Meanwhile, hydrogen bonding and π–π stacking interaction also exist during the adsorption process. The BB41 chemical structure consists of aromatic rings which permit possible various types of conjugations and favors the strong π–π stacking interaction. The aromatic hydrocarbon groups of CS that are detected by the FTIR spectrum may be

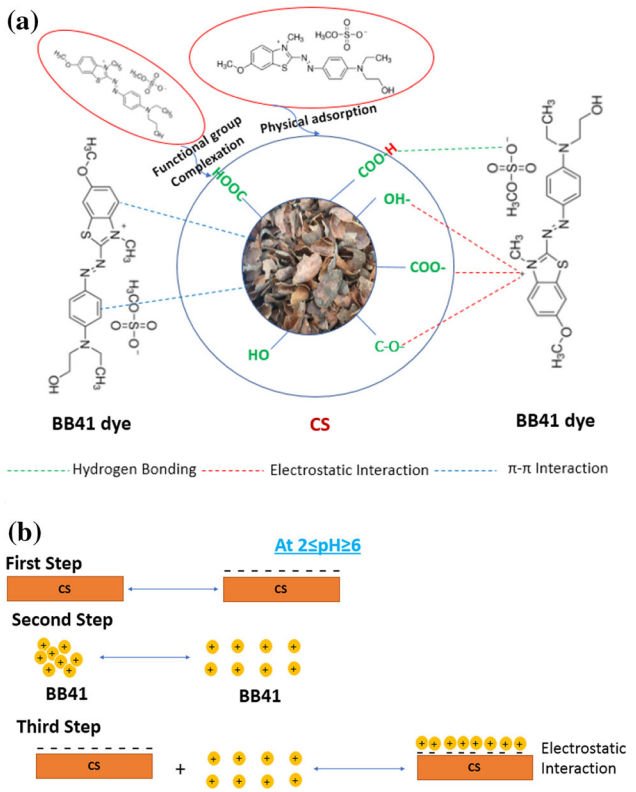

Fig. 5 **a** General proposed adsorption mechanism for the adsorption of BB41 dye over the CS adsorbent.; and **b** mechanism of adsorption from the point of solution pH for the removal of BB41 dye over the CS adsorbent

joined with the aromatic ring of BB41. BB41 dye has aromatic rings conjugated by one diazo bond (N=N). So, this mode of interaction can take place between the aromatic rings and –N=C–C=C– system for BB41 dye (Islam et al. 2018).

Furthermore, the pseudo-second-order kinetic model fits the experimental data of BB41 adsorption onto CS, suggesting that the chemical adsorption plays a significant role during the adsorption process. Meanwhile, the interaction between BB41 and CS involved physical mechanism that derived from the D-R model. Otherwise, the experimental results of the pH effect indicated that the electrostatic interaction mechanism affects the BB41 adsorption onto CS, but it is not the sole mechanism.

Moreover, the adsorption of BB41 molecules onto CS could occur through surface complexation and H^+ ions could be released into the solution. This mechanism can be confirmed at a low pH when cations are detected in the solution.

Furthermore, the stability of attraction and repulsion forces between the atoms is characterized by the sharing of electron pairs (delocalized electrons on the CS surface) between atoms (covalent bonds). This mechanism has a predominant effect over the electrostatic interaction as a result of the low intensity of oxygen groups that causes an increase in the π electron density, thus increase the adsorption potential caused by dispersive interactions (Ahmad et al. 2012).

In summary, the interaction between BB41 dye and CS referred to various mechanisms, including electrostatic interaction, hydrogen bonding, covalent bonding, physical interaction and π–π binding. A similar mechanism was also found by other researches (Albadarin et al. 2017; Li et al. 2016; Elessawy et al. 2020).

The adsorption (chemisorption) may take place until the surface function sites are fully occupied. Then, the dye molecules diffuse into the pores for further adsorption interactions. The suggested alteration in the BB41 adsorption mechanism onto the CS is shown in Fig. 5b according to the pH of the solution.

In the first stage, at acidic solutions ($2 \leq pH \leq 6$), various functional groups of CS such as C–O, –OH, and –COOH are existed (see Fig. 2g) and this stage is very fast. The second stage is the dissociation of agglomerated BB41 dye before adsorption which is slower than the first stage. The third stage is the electrostatic interaction between the negatively charged functional groups of CS and the positively charged tertiary ammonium of BB41 dye at this range of pH (See Figs. 2g, 3a). This stage should be the rate-determining step for adsorption of BB41 dye onto CS adsorbent although the second stage exhibited some importance to overall adsorption mechanism.

Conclusion

This study evaluated the CS performance in the BB41 removal from wastewater and optimized the operating variables of the adsorption process. The CS was characterized using different techniques such as SEM, EDX, FTIR, and XRD to investigate the CS surface morphology, elemental analysis, functional groups and crystallinity. The results elucidated that the CS surface is porous, rough, and its surface involves carboxylic and hydroxylic groups which gave a primary indication of the CS ability to be utilized as an adsorbent. The interaction between BB41 and CS referred to various mechanisms including electrostatic interaction, π–π stacking, hydrogen bonding, physical bonding and covalent bonding. Besides, the organic functional groups on the CS surface played an important role during the adsorption process. Due to the cocoa shells' low-cost, high efficiency, availability, technical and environmental benefits, it can be used as a promising adsorbent for dye removal from wastewater.

Acknowledgements The authors are deeply gratitude to both of Algiers University of Science and Technology Haouari Boumadiene

in Algeria and City of Scientific Research and Technological Applications (SRTA-City) in Egypt for supporting and facilitating this study.

References

Adebayo MA, Lima LDTP, Puchana-Rosero EC, Catalua MJ, Saucier R, Umpierres C, Vaghetti CS, Silva JCP, Ruggiero R (2014) Adsorption of Procion Blue MX-R dye from aqueous solutions by lignin chemically modified with aluminium and manganese. J Hazard Mater 268:43–50

Ahmad F, Daud WMAW, Ahmad MA, Radz R (2012) Cocoa (*Theobroma cacao*) shell-based activated carbon by CO_2 activation in removing of Cationic dye from aqueous solution: Kinetics and equilibrium studies. Chem Eng Res Des 90:1480–1490

Ahmad MA, Ahmad N, Bello OS (2015) Adsorption kinetic studies for the removal of synthetic dye using durian seed activated carbon. J Dispers Sci Technol 36:670–684

Albadarin AB, Collins MN, Naushad M, Shirazian S, Walker G, Mangwandi C (2017) Activated lignin-chitosan extruded blends for efficient adsorption of methylene blue. Chem Eng J 307:264–272

Ali RM, Hamad HA, Hussein MM, Malash GF (2016) Potential of using green adsorbent of heavy metal removal from aqueous solutions: adsorption kinetics, isotherm, thermodynamic, mechanism and economic analysis. Ecol Eng 91:317–332

Banerjee S, Sharma GC, Gautama RK, Chattopadhyaya MC, Upadhyay SN, Sharma YC (2016) Removal of Malachite Green, a hazardous dye from aqueous solutions using *Avena sativa* (oat) hull as a potential adsorbent. J Mol Liq 213:162–172

Bassyouni D, Mohamed M, El-Ashtoukhy E-S, El-Latif MA, Zaatout A, Hamad H (2019) Fabrication and characterization of electrospun Fe_3O_4/o-MWCNTs/polyamide 6 hybrid nanofibrous membrane composite as an efficient and recoverable adsorbent for removal of Pb(II). Microchem J 149:103998

Campos-Vega R, Nieto-Figueroa KH, Oomah BD (2018) Cocoa (*Theobroma cacao* L.) pod husk: renewable source of bioactive compounds. Trends Food Sci Technol 81:172–184

Cardoso NF, Lima EC, Pinto IS, Amavisca CV, Royer B, Pinto RB, Alencar WS, Pereira SFP (2011) Application of cupuassu shell as biosorbent for the removal of textile dyes from aqueous solution. J Environ Manag 92:1237–1247

Conrad EK, Nnaemeka OJ, Chris AO (2015) Adsorptive removal of methylene blue from aqueous solution using agricultural waste: equilibrium, kinetic and thermodynamic studies. Am J Chem Mater Sci 2:14–25

El Essawy NA, Ali SM, Farag HA, Konsowa AH, Elnouby M, Hamad HA (2017) Green synthesis of graphene from recycled PET bottle wastes for use in the adsorption of dyes in aqueous solution. Ecotoxicol Environ Saf 145:57–68

Elessawy NA, El-Sayed EM, Ali S, Elkady MF, Elnouby M, Hamad HA (2020) One-pot green synthesis of magnetic fullerene nanocomposite for adsorption characteristics. J Water Process Eng 34:101047

Elhafez SEA, Hamad HA, Zaatout AA, Malash GF (2017) Management of agricultural waste for removal of heavy metals from aqueous solution: adsorption behaviors, adsorption mechanisms, environmental protection and techno-economic analysis. Environ Sci Pollut Res 24:1397–1415

Elkady M, Shokry H, El-Sharkawy A, El-Subruiti G, Hamad H (2019) New insights into the activity of green supported nanoscale zero-valent iron composites for enhanced acid blue-25 dye synergistic decolorization from aqueous medium. J Mol Liq 254:111628

Gupta VK, Agarwal S, Olgun A, Demir HI, Yola ML, Atar N (2016) Adsorptive properties of molasses modified boron enrichment waste based nanoclay for removal of basic dyes. J Ind Eng Chem 34:244–249

Hamad H, Abd El-latif M, Kashyout A, Sadik W, Feteha M (2015) Synthesis and characterization of core–shell–shell magnetic ($CoFe_2O_4$–SiO_2–TiO_2) nanocomposites and TiO_2 nanoparticles for the evaluation of photocatalytic activity under UV and visible irradiation. New J Chem 39:3116–3128

Hamad H, Bailón-García E, Morales-Torres S, Pérez-Cadenas AF, Carrasco-Marín F, Maldonado-Hódar FJ (2018) Physicochemical properties of new cellulose-TiO_2 composites for the removal of water pollutants: developing specific interactions and performances by cellulose functionalization. J Environ Chem Eng 6:5032–5041

Hassaan MM, Pantaleo A, Tedone L, Elkatory MR, Ali RM, El Nemr A, De Mastro G (2019) Enhancement of biogas production via green ZnO nanoparticles: experimental results of selected herbaceous crops. Chem Eng Commun. https://doi.org/10.1080/00986445.2019.1705797

Islam MT, Saenz-Arana R, Hernandez C, Guinto T, Ahsan MA, Bragg DT, Wang H, Alvarado-Tenorio B, Noveron JC (2018) Conversion of waste tire rubber into a high-capacity adsorbent for the removal of methylene blue, methyl orange, and tetracycline from water. J Environ Chem Eng 6:3070–3082

Jogihalli P, Singh L, Kumar K, Sharanagat VS (2017) Novel continuous roasting of chickpea (*Cicer arietinum*): study on physico-functional, antioxidant and roasting characteristics. Food Technol 86:456–464

Kamel DA, Farag HA, Amin NK, Zatout AA, Ali RM (2018) Smart utilization of jatropha (*Jatropha curcas* Linnaeus) seeds for biodiesel production: optimization and mechanism. Ind Crop Prod 111:407–413

Keskinkan O, Göksu MZL (2007) Assessment of the dye removal capability of submersed aquatic plants in a laboratory-scale wetland system using ANOVA. BJChE 24:193–202

Khamparia S, Jaspal DK (2017) *Xanthium strumarium* L. seed hull as a zero cost alternative for Rhodamine B dye removal. J Environ Manag 197:498–506

Kooli F, Liu Y, Abboudi M, Hassani HO, Rakass S, Ibrahim SM, Wadaani FA (2019) Waste bricks applied as removal agent of basic blue 41 from aqueous solutions: base treatment and their regeneration efficiency. Appl Sci 9:1237

Kumar KV, Sivanesan S (2006) Isotherm parameters for basic dyes onto activated carbon: comparison of linear and non-linear method. J Hazard Mater B129:147–150

Kyzas GZ, Lazaridis NK, Bikiaris DN (2013) Optimization of chitosan and β-cyclodextrin molecularly imprinted polymer synthesis for dye adsorption. Carbohydr Polym 91:198–208

Li G, ZhuW ZC, Zhang S, Liu L, Zhu L, Zhao W (2016) Effect of a magnetic field on the adsorptive removal of methylene blue onto wheat straw biochar. Bioresour Technol 206:16–22

Lim LBL, Priyantha N, Zehra T, Then CW, Chan CM (2016) Adsorption of crystal violet dye from aqueous solution onto chemically treated *Artocarpus odoratissimus* skin: equilibrium, thermodynamics, and kinetics studies. Desalination Water Treat 57:10246–10260

Monteiro MS, Farias RFD, Chaves JAP, Santana SA, Silva HAS, Bezerra CWB (2017) Wood (*Bagassa guianensis* Aubl) and green coconut mesocarp (*Cocos nucifera*) residues as textile dye removers (Remazol Red and Remazol Brilliant Violet). J Environ Manag 204:23–30

Pua FL, Sajab MS, Chia CH, Zakaria S, Abdul Rahman I, Salit MS (2013) Alkaline-treated cocoa pod husk as adsorbent for removing methylene blue from aqueous solutions. J Environ Chem Eng 1:460–465

Roy P, Mondal NK, Bhattacharya S, Das B, Das K (2013) Removal of arsenic (III) and Arsenic (V) on chemically modified low-cost adsorbent: batch and column operations. Appl Water Sci 3:293–309

Shokry H, Elkady M, Hamad H (2019) Nano activated carbon from industrial mine coal as adsorbents for removal of dye from simulated textile wastewater: operational parameters and mechanism study. J Mater Res Technol 8:4477–4488

Singh H, Chauhan G, Jain AK, Sharma SK (2017) Adsorptive potential of agricultural wastes for removal of dyes from aqueous solutions. J Environ Chem Eng 5:122–135

Thirunavukkarasu A, Muthukumaran K, Nithya R (2018) Adsorption of acid yellow 36 onto green nanoceria and amine functionalized green nanoceria: comparative studies on kinetics, isotherm, thermodynamics, and diffusion analysis. J Taiwan Inst Chem Eng 93:211–225

Wang H, Xie R, Zhang J, Zhao J (2018) Preparation and characterization of distillers' grain based activated carbon as low cost methylene blue adsorbent: mass transfer and equilibrium modeling. Adv Powder Technol 29:27–35